Supporting Information

The global motion affecting electron transfer of *Plasmodium falciparum* type II NADH dehydrogenases: a novel non-competitive mechanism of quinoline ketone derivative inhibitors

Tao Xie, †[a] Zhixiang Wu, †[a] Jinke Gu, [b] Runyu Guo, [b] Xiao Yan, [a] Huaichuan Duan, [a] Xinyu Liu, [c] Wei Liu, [a] Li Liang, [a] Hua Wan, [d] Yafei Luo, [e] Dianyong Tang, [e] Hubing Shi, *[c] and Jianping Hu, *[a]

[a.] *College of Pharmacy and Biological Engineering, Sichuan Industrial Institute of Antibiotics, Key Laboratory of Medicinal and Edible Plants Resources Development of Sichuan Education Department, Chengdu University, Chengdu, 610106, China.*

[b.] *Ministry of Education Key Laboratory of Protein Science, Tsinghua-Peking Joint Center for Life Sciences, Beijing Advanced Innovation Center for Structural Biology, School of Life Sciences, Tsinghua University, Beijing, 100084, China.*

[c.] *Laboratory of Tumor Targeted and Immune Therapy, Clinical Research Center for Breast, West China Hospital, Sichuan University, Chengdu, 610106, China.*

[d.] *College of Mathematics and Informatics, South China Agricultural University, Guangzhou,510642, China.*

[e.] *Chongqing Key Laboratory of Environmental Materials and Remediation Technology, Chongqing University of Arts and Sciences, Chongqing, 402160, P. R. China.*

* *Corresponding authors: shihb@scu.edu.cn(H.S.); hjpcdu@163.com (J.H.); Tel.: +86-28-8461-6301 (J.H.)*

† *These authors contributed equally to this work.*

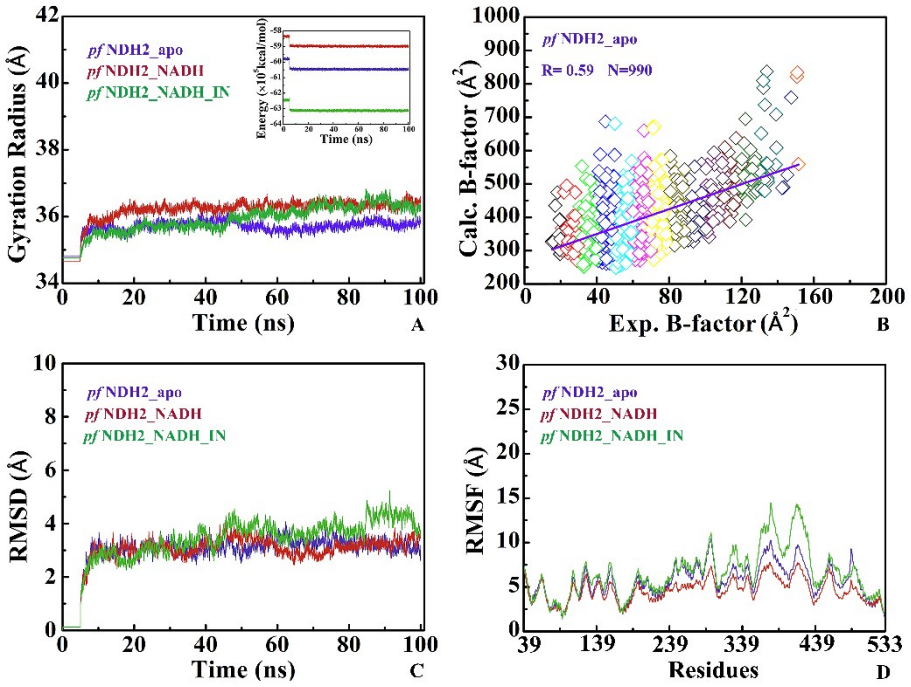

Fig. S1 The convergence behavior of the three comparative MD simulations: the variations of radius gyration and potential energy (the upper right) over simulation time (A), the correlation of experimental B-factors with calculation data (B), the RMSD variations over simulation time (C) and the RMSF distribution (D).

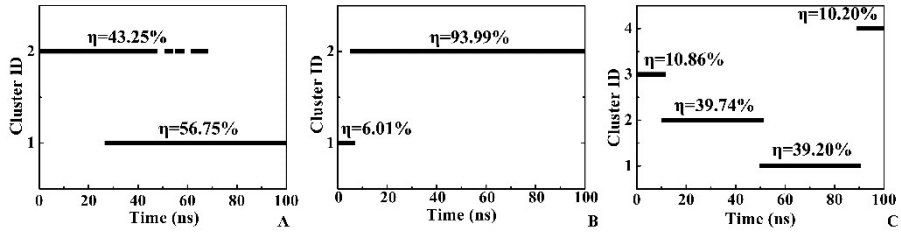

Fig. S2 Conformational cluster analyses of *pf*NDH2_apo (A), *pf*NDH2_NADH (B) and *pf*NDH2_NADH_IN (C), where η represents the conformational proportion of each cluster.

Distance（Å）	Residues
2.5-3.0	P434,**L473**, **T211**, P210
3.0-3.5	**V278**,**S309**,**E214**,G245,G207, E244
3.5-4.0	Y277,G209,Y276,V206,G310,G208,A308
4.0-4.5	P251,W307,A474,S472,I243,I157,E214,D354
4.5-5.0	F155,L311,T252,D354,L250,Y276,V213,

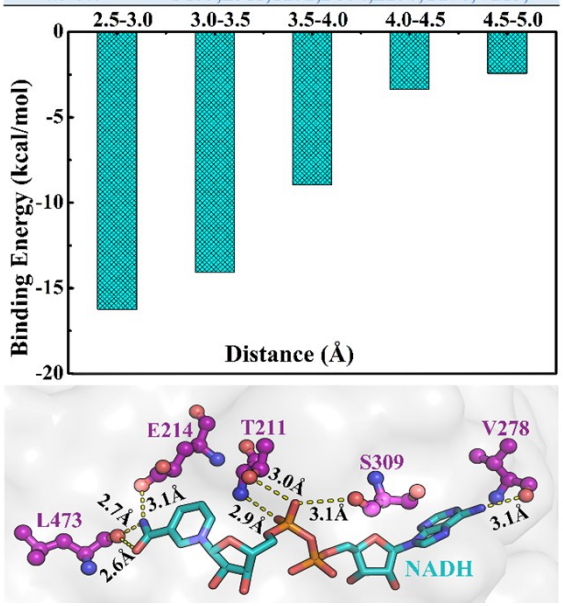

Fig. S3 A schematic illustration of NADH molecular recognition. The top form lists the key residues at different distances around NADH; the middle histogram shows the sum of binding energy over different distance scopes; the lower inset displays the binding model of NADH with *pf*NDH2, where stick model represents NADH, and key residues are described with ball-stick model.

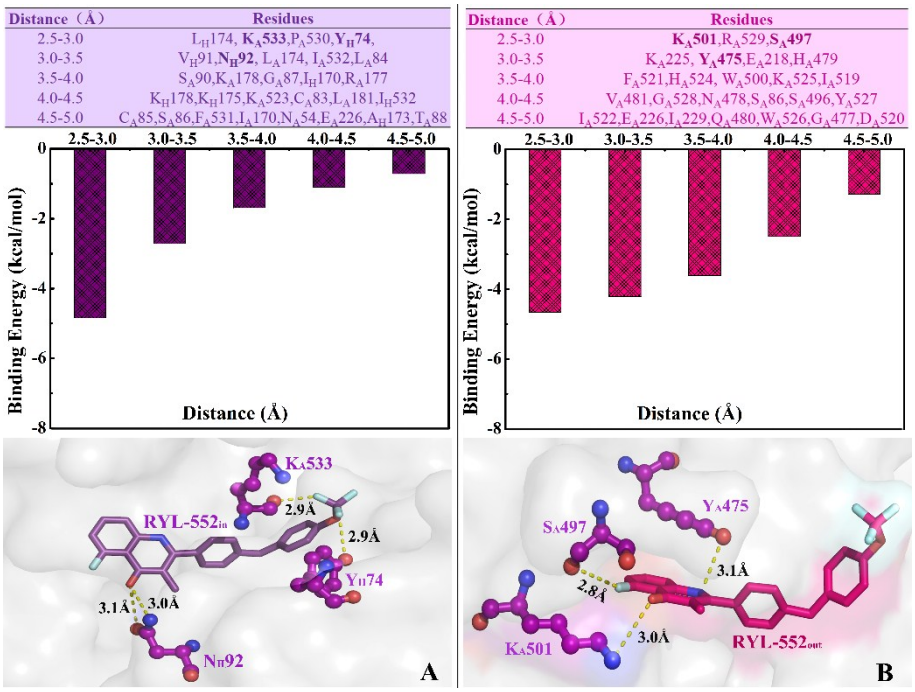

Fig. S4 A schematic illustration of RYL-552$_{in}$ (A) and RYL-552$_{out}$ (B) molecular recognition, where the subscript of A and H represents chain A and chain H of *pf*NDH2. The top form lists the key residues at different distances around RYL-552$_{in}$/ RYL-552$_{out}$; the middle histogram shows the sum of binding energy over different distance scopes; the lower inset displays binding model of RYL-552$_{in}$/ RYL-552$_{out}$, where stick model represents RYL-552$_{in}$/ RYL-552$_{out}$, and key residues are described with ball-stick model.

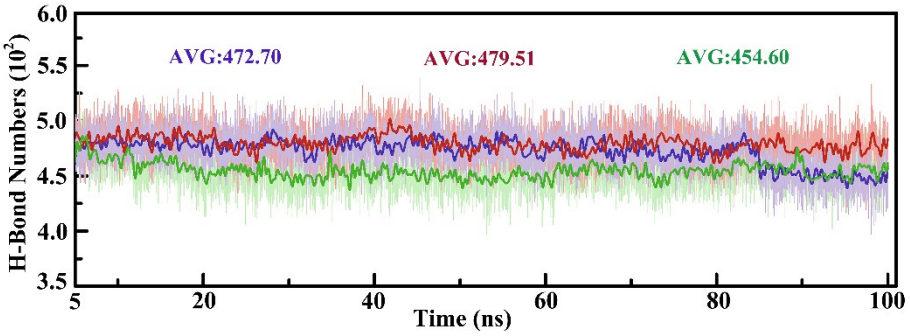

Fig. S5 The total number of hydrogen bonds in *pf*NDH2_apo (purple), *pf*NDH2_NADH (red) and *pf*NDH2_NADH_IN (green) during the unconstrained MD simulation (5-100 ns).

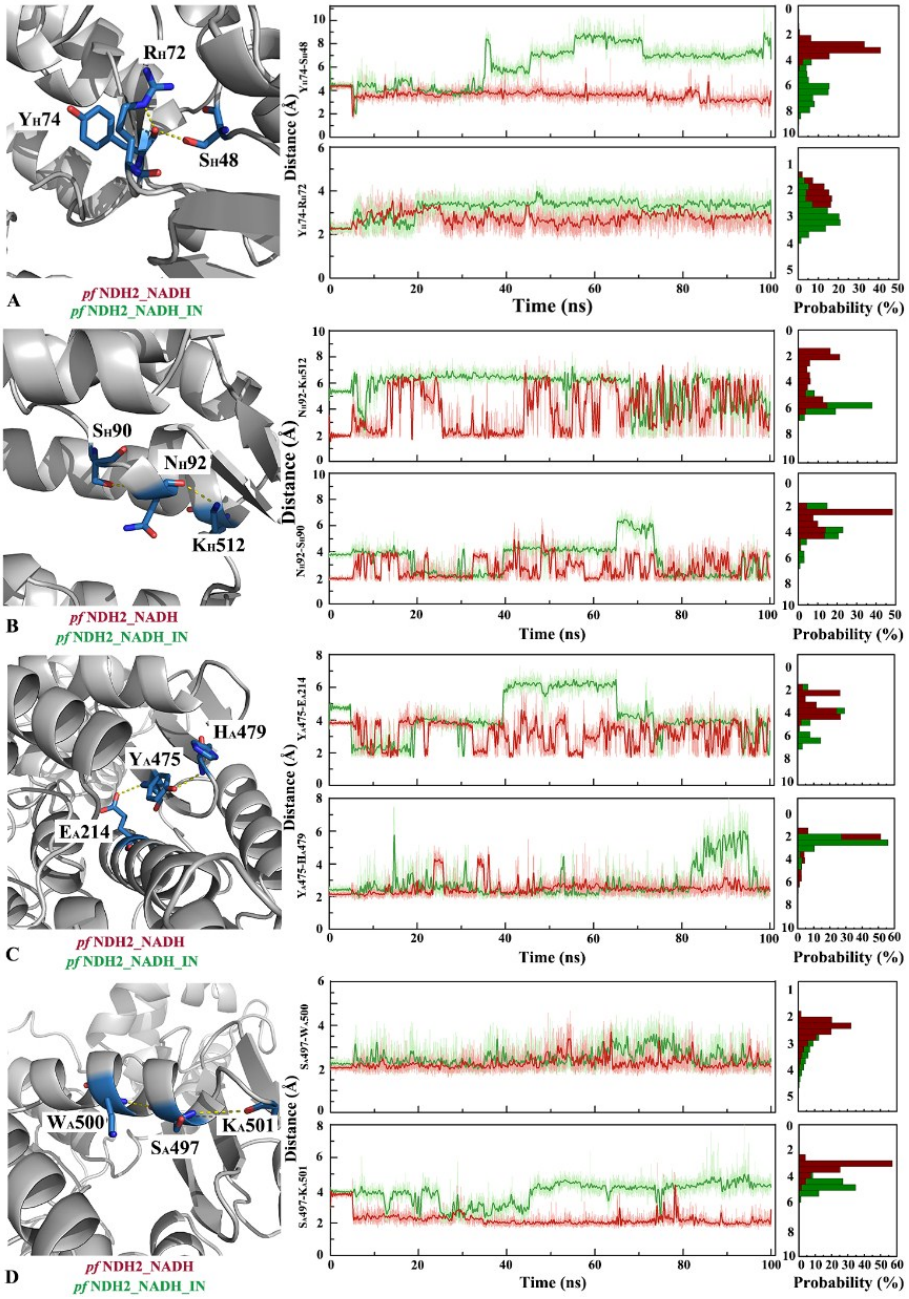

Fig. S6 The distance variation between key residues in *pf*NDH2_NADH and *pf*NDH2_NADH_IN, where subscript A/ H represent chain A / H of *pf*NDH2. The left inset shows the positional information of Y_H74, R_H72, S_H48, N_H92, S_H90, K_H512, Y_A475, H_A479, E_A214, S_A497, W_A500 and K_A501 in *pf*NDH2_NADH; the middle inset displays a series of distance variations over simulation time; the right inset reveals probability distribution of the corresponding distance.

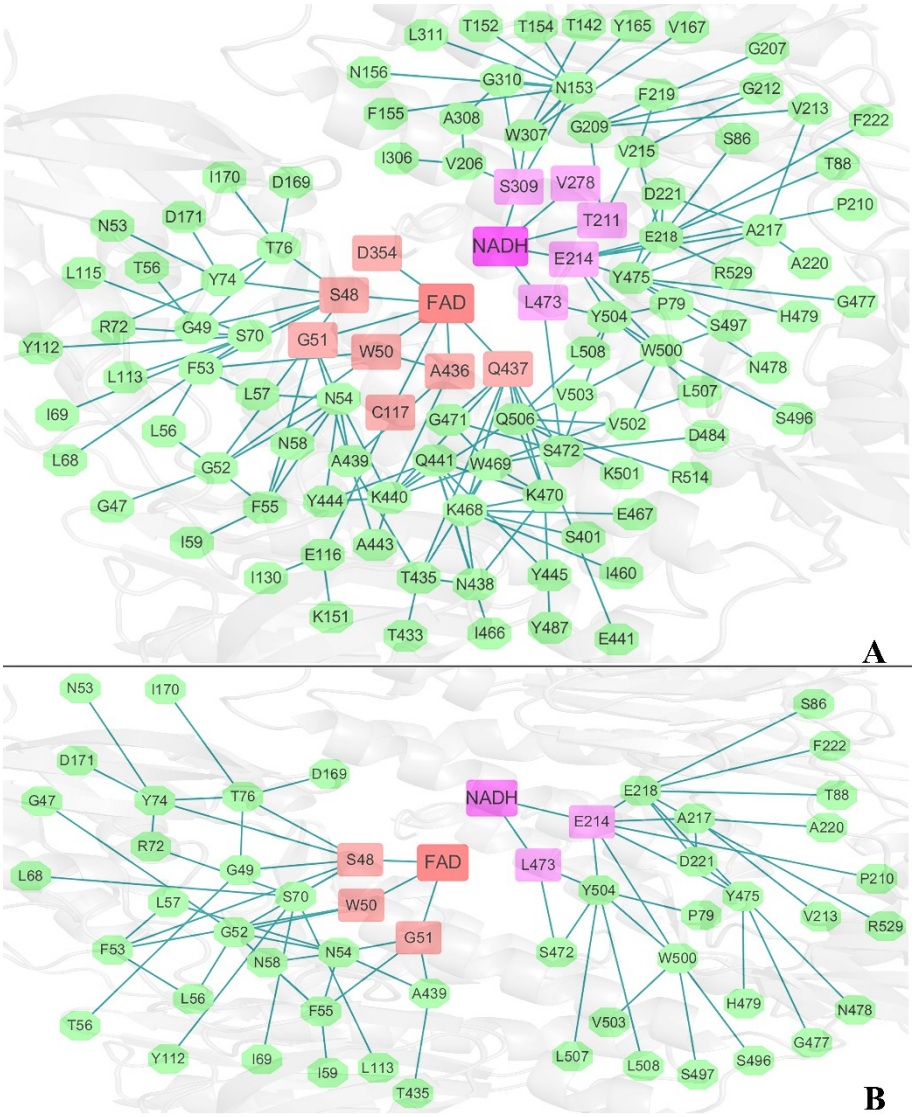

Fig. S7 The hydrogen bonds network in the range of 12 Å around FAD and NADH in *pf*NDH2_NADH_IN (A). Red and purple colors are used to represent the key residues around FAD and NADH, respectively. The hydrogen bonds network in the range of 12 Å around FAD and NADH in *pf*NDH2_NADH (B). Red and purple colors are used to represent the key residues around FAD and NADH, respectively.

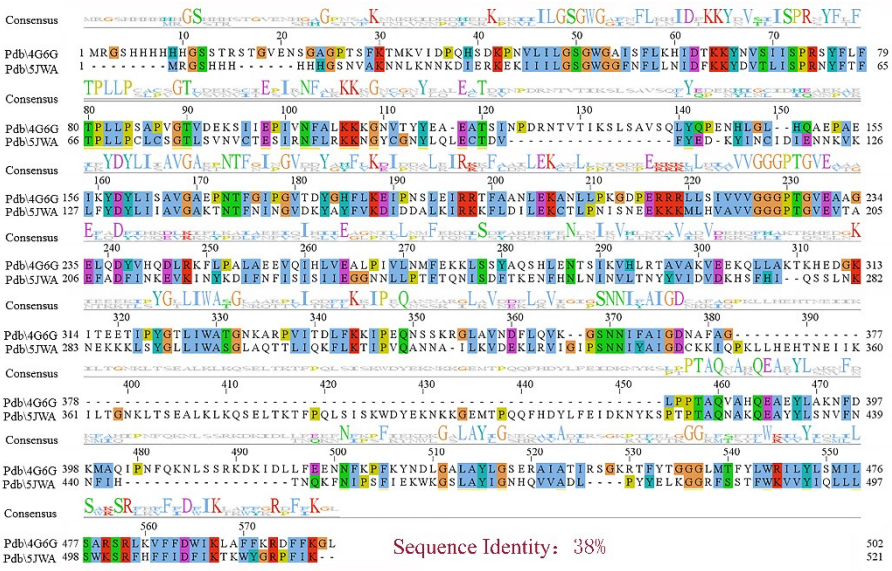

Fig. S8 The sequence alignment of *pf*NDH2 (PDB ID: 5JWA) with yeast type II NADH-Ubiquinone oxidoreductase (PDB ID: 4G6G).

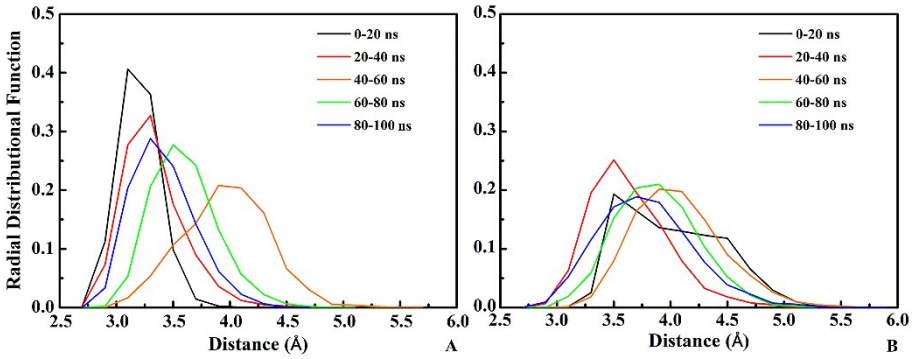

Fig. S9 Radial distribution function (RDF) graphs of distances between FAD-N5 and NADH-C4 in the *pf*NDH2_NADH (A) and *pf*NDH2_NADH_IN (B) systems.

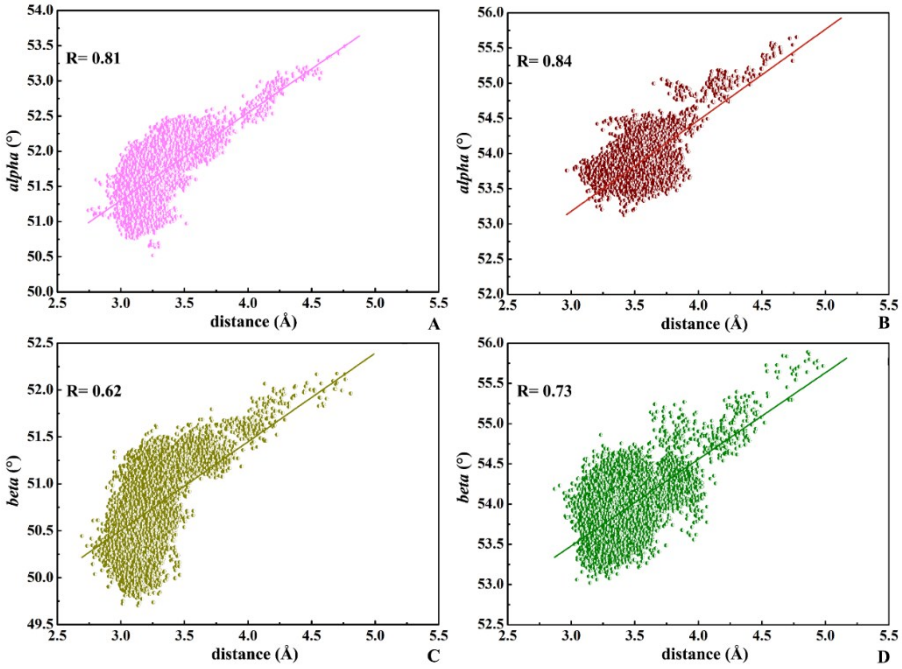

Fig. S10 A represents the correlation between the distance of FAD-N5 with NADH–C4 and the intramolecular angle *alpha* in *pf*NDH2_NADH (R= 0.81); B shows the correlation between the distance of FAD-N5 with NADH–C4 and the intramolecular angle *alpha* in *pf*NDH2_NADH_IN (R= 0.84); C displays the correlation between the distance of FAD-N5 with NADH–C4 and the intramolecular angle *beta* in *pf*NDH2_NADH (R= 0.62); D reveals the correlation between the distance of FAD-N5 with NADH–C4 and the intramolecular angle *beta* in *pf*NDH2_NADH_IN (R= 0.73).